Mon. Not. R. Astron. Soc. **280,** 1062–1070 (1996)

The spectral energy distribution and mass-loss history of IRC + 10420

René D. Oudmaijer,[1,2] M. A. T. Groenewegen,[3] H. E. Matthews,[4,5] J. A. D. L. Blommaert[6]★ and K. C. Sahu[7]

[1]*Kapteyn Astronomical Institute, PO Box 800, NL-9700 AV Groningen, The Netherlands*
[2]*Imperial College of Science, Technology and Medicine, Blackett Laboratory, Prince Consort Road, London SW7 2BZ*
[3]*Max-Planck-Institut für Physik and Astrophysik, Karl-Schwarzschild Straße 1, D-85740 Garching, Germany*
[4]*Joint Astronomy Centre, 660 N. A'ohōkū Place, Hilo, HI 96720, USA*
[5]*Herzberg Institute of Astrophysics, National Research Council of Canada, Ottawa, Ontario K1A 0R6, Canada*
[6]*Institut d'Astrophysique de Paris, CNRS, 98 bis Bd. Arago, F-75014, Paris, France*
[7]*Space Telescope Science Institute, 3700 San Martin Drive, Baltimore, MD 21218, USA*

Accepted 1996 January 2. Received 1995 December 15; in original form 1995 July 31

ABSTRACT

We present a study of the spectral energy distribution of the peculiar hypergiant IRC + 10420. To this end we have collected published photometry of IRC + 10420 and obtained some new data, in order to construct the spectral energy distribution and fit it with a radiative transfer model. In addition high-quality ^{12}CO spectra of the rotational $J = 1–0$, 2–1, 3–2 and 4–3 transitions have been obtained to determine the gas outflow velocity and independently estimate the gas mass-loss rate.

The main conclusions from this work are that the photometric changes over the last 20 years indicate that the object has increased in temperature by more than 1000 K and that the spectral energy distribution cannot be fitted with a single-shell model without first including a hot component. This hot component is likely to be a circumstellar disc. Finally, we present evidence that IRC + 10420 is not a post-AGB star.

Key words: stars: AGB and post-AGB – circumstellar matter – stars: evolution – stars: individual: IRC + 10420 – stars: mass-loss – supergiants.

1 INTRODUCTION

The hypergiant IRC + 10420 ($19^h24^m26\overset{s}{.}7 + 11^d15^m10\overset{s}{.}9$ epoch 1950.0) is a peculiar star. The object exhibits a large far-infrared excess attributed to circumstellar dust, making it one of the brightest sources in the *IRAS* Point Source Catalog, and was one of the earliest known 'warm' central stars associated with an OH maser (Giguere, Woolf & Webber 1976).

Two explanations for the nature of IRC + 10420 have been put forward in the literature. The first is that IRC + 10420 is a post-AGB star. Indeed, in many respects IRC + 10420 resembles the group of 'optically bright post-AGB stars' (Kwok 1993; Waters, Waelkens & Trams 1993a). These are low-to-intermediate mass stars that have evolved off the asymptotic giant branch (AGB) and are in the transition to the planetary nebula phase. The sample of optically bright post-AGB objects mainly consists of G–A-type supergiants surrounded by a cool dust shell, from which OH maser emission has often been detected (te Lintel-Hekkert, Chapman & Zijlstra 1992).

However, over the last years evidence has been growing that IRC + 10420 is in fact a massive star. The inferred distance of 3–5 kpc to IRC + 10420 led people to place IRC + 10420 in the upper part of the Hertzsprung–Russell (HR) diagram, where it should be evolving from the red supergiant phase to the Wolf–Rayet (WR) phase (Humphreys 1991; Nedoluha & Bowers 1992; Jones et al. 1993, hereafter J93). A distance of 5 kpc (J93; Nedoluha & Bowers 1992) places IRC + 10420 on evolutionary tracks computed for stellar masses of 20–40 $M_\odot$ (see, e.g., Schaller et al. 1992, and references therein). Although several F–G hypergiants are known, IRC + 10420 is the only one with a significant infrared flux, indicating large mass-loss rates in a previous red supergiant phase. This makes the object unique for the study of massive star evolution, and implies

★Present address: ISO Science Operations Centre, Astrophysics Division, Villafranca del Castillo Satellite Tracking Station, PO Box 50727, 28080, Madrid, Spain.

that IRC +10420 is caught in the transition between OH/IR supergiants and WR stars. Recently, Kastner & Weintraub (1995) proposed that the G supergiant HD 179821 may be another example of such an object.

The main aim of this paper is to derive the mass-loss rate in the previous mass-loss phase. If IRC +10420 is a post-red supergiant, such information is extremely important for the understanding of the evolution of high-mass stars.

To this end, we have collected published photometry of IRC +10420 and obtained some new data, in order to construct the spectral energy distribution and fit it with a radiative transfer model. High-quality ^{12}CO spectra of the 1–0, 2–1, 3–2 and 4–3 transitions have been obtained to determine the gas outflow velocity and independently estimate the gas mass-loss rate.

The outline of this paper is as follows. In Section 2 the spectral energy distribution will be constructed, where the drastic changes in the photometric behaviour of IRC +10420 will be discussed in terms of an increasing temperature of the object. In Section 3 the CO spectroscopy will be presented, and the findings of Sections 2 and 3 will be used as input in Section 4, where the spectral energy distribution of IRC +10420 will be fitted with a radiative transfer code. The results are discussed in Section 5, and we conclude in Section 6.

2 THE SPECTRAL ENERGY DISTRIBUTION OF IRC +10420

2.1 New photometry

IRC +10420 was observed on 1994 April 23 with the 80-cm telescope of Observatorio del Teide, operated by Instituto de Astrofísica de Canarias (IAC), Tenerife. One CCD exposure of 5 min was taken in the Johnson *V* band. For calibrations, two exposures of a nearby field containing the stars L111–773 and L111–775 were taken. The observed *V* magnitude of IRC +10420 was found to be 11.03 ± 0.02 mag.

Near-infrared photometry was obtained on several occasions with the 1.5-m Carlos Sanchez Telescope at Observatorio del Teide of IAC, Tenerife. The photometer is a single-channel photometer equipped with a liquid-nitrogen-cooled InSb detector, coupled to a focal plane chopper. Standard *JHKL'M* filters are used (details of this photometric system are described by Alonso, Arribas & Martinez-Roger 1994). An aperture of 15-arcsec diameter was used during these observations. The sky background is corrected by means of a chopper which works at a frequency of 8 Hz and a chopper throw of 30 arcsec. To correct for any gradient in the sky brightness, the background is observed on both sides of the object and the mean is used. Three cycles of observations in each filter, each with an effective integration time of 1 min, were usually taken to check the consistency of the observations. The final value is the mean of these three cycles of observations. In the week of 1993 August 25–31 IRC +10420 was observed four times, an additional measurement was made in 1994 April. The newly obtained photometry is listed in Table 1.

2.2 Photometric variability

Despite the large number of near-infrared photometrical measurements, optical photometry is sparse. It is surprising that the *V* magnitude of this well-studied object reported in the previous section is only the third *V*-band measurement since 1973, in the paper documenting the discovery of IRC +10420 (Humphreys et al. 1973). The *V* magnitudes are identical within the expected errors of ~0.1 mag over the last 20 years, the NIR photometry, however, is highly variable; between 1974 and ~1980 IRC +10420 decreased in brightness by about 0.75 mag, and after that the NIR magnitudes varied erratically within 0.2 mag as noted by J93 and noticeable in Fig. 1.

J93 show the evolution of the broad-band *K* magnitude with time, and conclude that thermally reradiating hot dust, located close to the star, has moved away from the star during these 20 years, giving rise to a decrease in flux, at first, at the near-infrared wavelengths and later at longer wavelengths.

In Fig. 1 we show all *V*, *J* and *K* measurements (not corrected for the different systems) listed in J93, with the new points added. Since no errors are given in the original photometry and different systems are used, the errors in the data points may be of order 0.1 mag. This is still smaller than the symbols in the figure indicating that the changes are real. The *V* magnitude has remained essentially constant, while both the *J* and *K* magnitudes show an increase of 0.75 mag in the period 1975–83. After this rise, the magnitudes vary with an amplitude of about 0.2 mag. Note that the

Table 1. New photometry of IRC +10420.

Date	*V*	*J*	*H*	*K*	*L'*
λ (μm)	0.55	1.258	1.647	2.205	3.830
August 25 1993		5.45±0.02	4.45±0.03	3.37±0.03	1.02±0.09
August 28 1993		5.51±0.07	4.50±0.02	3.52±0.05	1.06±0.03
August 30 1993		5.55±0.01	4.50±0.02	3.50±0.02	1.04±0.04
August 31 1993		5.50±0.01	4.46±0.01	3.48±0.01	1.04±0.04
April 5 1994		5.34±0.03	4.36±0.03	3.33±0.03	0.98±0.03
April 23 1994	11.03 ± 0.02				

decrease of the J and K magnitudes occurs in a period in which the emergence of hydrogen emission lines has been found by Oudmaijer et al. (1994).

From the plot it is clear that the J magnitude has increased simultaneously with the K band. If this were the result of an expanding dust shell, strong excess emission should have been present at the J band in 1974. A simple way to determine the possible excess flux at J is by fitting Kurucz (1979) atmospheric models to the spectral energy distribution (SED). We therefore constructed two photometric data sets from the available photometry. Bearing the variability in mind, we used only the most recent measurements listed by J93, *VRI* photometry for 1991 October and two sets of near-infrared O'Brien photometry obtained in 1992 March and April. The conversion from the magnitude to the flux scale was performed using the tables by Ney, Strecker & Gehrz (1973). This set will be denoted the '1992' set (see also Section 2.4).

It turned out that it was possible to construct an almost simultaneously observed spectral energy distribution for 1974 ('the 1974 set'). These are the optical 13-colour photometry by Craine et al. (1976), and two near-infrared sets from the O'Brien system observed in 1974 July and November (listed by J93). For the latter two sets, we have taken the logarithmic mean of the two measurements. Craine et al. list a different zero-magnitude flux at V than does the original paper on the 13-colour system published by Johnson & Mitchell (1975), where the zero-magnitude flux density is 8 per cent lower. We used the latter value.

The 1974 and 1992 energy distributions of IRC +10420 are plotted in Fig. 2, along with the best-fitting Kurucz models in the 0.4–1.4 μm wavelength range. If the J band is rejected from the fitting procedure, the results are very similar.

Several things are apparent from the plot; the J magnitude is entirely photospheric at both epochs. It is not possible to obtain a reasonable fit to the optical data and obtain an excess flux at J. Thus, the J magnitude is a measure of the photospheric flux at 1.25 μm. Secondly, the excess emission at the K band, which traces hot dust, is 0.75 mag at both epochs. It is hard to envisage the decrease at the K band, owing to an expanding dust shell, while the excess at K remained the same. Thirdly, by fitting Kurucz models to an SED, there are essentially two free parameters, the effective temperature and the circumstellar and insterstellar extinction, $E(B-V)$, for which the formulation by Savage & Mathis (1979) is used.

For the 1974 energy distribution, we fitted the SED for $T_{\rm eff}=6000$ and 6500 K, where the temperature range was more or less restricted to the spectral type F8 determined by Humphreys et al. (1973) from spectra obtained in the early seventies. The situation is not so clear for the 1992 data, and we used temperatures from 6000 to 7500 K for the Kurucz models. The large extinction suffered by the photosphere at different temperatures cancelled out in such a way that good fits could be obtained for temperatures between 6000 and 7500 K, with increasing $E(B-V)$ values for higher temperatures. All fits have about the same quality: the fitted $E(B-V)$ values for the different $T_{\rm eff}$ are listed in Table 2, and some fits are shown in Fig. 2. Note the lower $E(B-V)$ for the 6000-K fit to the 1992 SED, compared with the 6000-K fit to the 1974 data.

2.3 Decreasing luminosity or constant luminosity

In the above section, we confirm the change in the K band found by J93. It appears, however, that their explanation for the decrease in terms of an expanding dust shell is not correct. From fits to the data, we find that the excess emission at K compared to the photosphere has remained the same over 20 years, while a similar change at the J band is found, where no excess emission is observed.

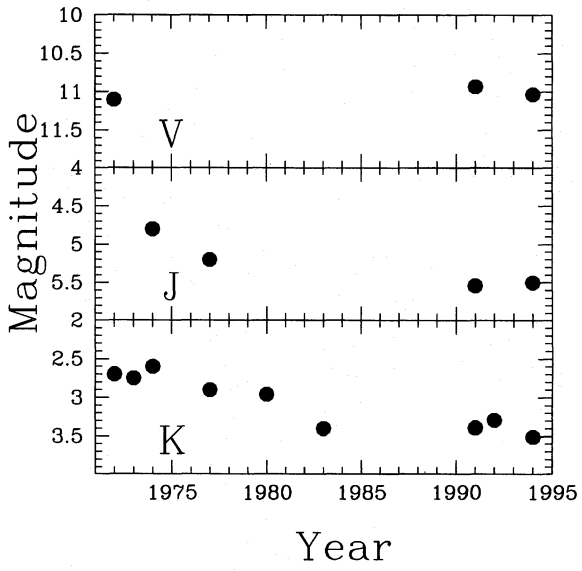

Figure 1. The V, J and K magnitudes are plotted versus time. The errors are smaller than the plot symbols.

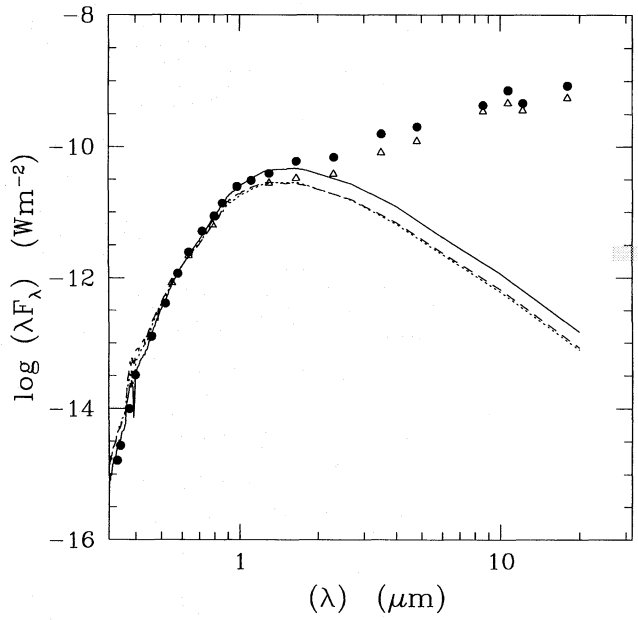

Figure 2. Photometry of IRC +10420 in 1974 (circles) and in 1992 (triangles). The solid line represents a Kurucz model fit to the 1974 data, while the dashed and dotted lines represent Kurucz fits of 7500 and 6000 K respectively to the 1992 data. The latter fits are almost identical.

Table 2. Best-fitting Kurucz models to the photometry.

		1974	1992
T_{eff}	log g	$E(B-V)$	$E(B-V)$
6000	0.5	2.33	2.08
6500	1.0	2.47	2.18
7000	1.0		2.28
7500	1.0		2.41

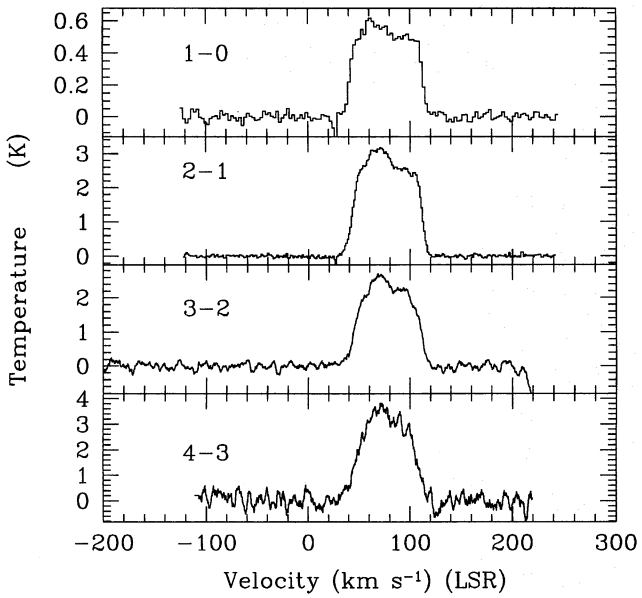

Figure 3. The observed spectra, corrected to the local standard of rest. The temperatures are on a main-beam scale. Note the blue excess emission that is visible in all spectra.

Another finding is that the reddening towards IRC +10420 apparently has decreased between the two epochs if the temperature has remained constant; for the 1974 6000-K model an $E(B-V)=2.33$ is found, while for the 1992 6000-K fit an $E(B-V)=2.08$ is determined. The errors in the derived $E(B-V)$ are quite small; changing this parameter by 0.05 results in significantly worse fits.

The fact that the extinction at V [$A_V=3.1\times E(B-V)$] has decreased by ≈ 0.75 mag is in contrast to the observation that the V magnitude remained constant. If the temperature of IRC +10420 was 6000 K at both epochs then, in order to counterbalance the decrease in extinction, the V magnitude (and thus the bolometric magnitude) should have become fainter by about 0.75 mag. In this case the decrease in bolometric magnitude is traced by the change in the J and K bands, where the extinction is less severe than at the V band. This scenario (constant T_{eff}, decrease in bolometric luminosity) requires a simultaneous decrease of the circumstellar extinction, tuned such that the decrease in A_V would almost exactly equal the decrease in bolometric luminosity.

Perhaps a simpler explanation for the observed changes is a change in stellar temperature while the bolometric luminosity and the extinction (circumstellar + interstellar) remain the same. The decrease in the near-infrared is then explained by a shift of the peak of the energy distribution to shorter wavelengths. From Table 2 we find that the reddening would have remained essentially constant had the temperature increased from 6000 K in 1974 to ~7000–7500 K in 1992. The constancy of the V magnitude can be understood from the fact that the bolometric correction for objects between 6000 and 7500 K is close to zero.

One can also look at the intrinsic colours for F-type supergiants: from the tables of Koornneef (1983) we find that the intrinsic $V-K$ colour is 1.21 for an F8 supergiant, 0.93 for an F5 supergiant, 0.75 for an F2 supergiant and 0.63 for an F0 supergiant. The bolometric correction for F-type supergiants is approximately 0, so that, assuming $E(B-V)$ remained constant, the increase of ~0.75 mag in K can be almost entirely explained from the change in intrinsic colour (0.6 mag from F8 to F0).

The increase in temperature is further supported by the spectra of Oudmaijer, Waters & Geballe (1995), who found significant changes over the last 20 years in the optical spectrum of IRC +10420. From a comparison of the blue spectrum of IRC +10420 with several standards, they conclude that the spectral type of IRC +10420 is late A. The spectral type of IRC +10420 was determined by Humphreys et al. in 1974 to be F8I$^+$. Both the photometry and the spectral type classification are an independent confirmation of the interpretation that IRC +10420 has increased its temperature by about 1000 K over the last 20 years.

2.4 Completing the 1992 SED

In order to fit a dust model through the SED of IRC +10420, the 1992 energy distribution is complemented with Kuiper Airborne Observatory photometry obtained by J93 in 1991 June, the *IRAS* far-infrared measurements and 1.3-mm photometry listed in Walmsley et al (1991).

The *IRAS* Low Resolution Spectrum was extracted using the *IRAS* GIPSY software available at Space Research Groningen (Wesselius et al. 1992; van der Hulst et al. 1992; Assendorp et al. 1995). Four scans, two by the short-wavelength detector and two by the long-wavelength detector, were usable. A third long-wavelength detector scan was deviant from the others, and it was decided to reject it from further processing during the extraction process. To align the short-wavelength spectrum with the long-wavelength LRS spectrum, the blue spectrum was scaled up to 40 per cent. The agreement between the LRS spectrum and the mid-IR KAO photometry is excellent (see Fig. 4).

3 CO OBSERVATIONS

Observations of the CO rotational $J=3$–2 and 4–3 transitions at 345 and 461 GHz, respectively, were made with the 15-m JCMT on 1993 June 7 and 3. For both measurements, facility single-channel SIS mixer receivers were used (see Matthews 1995, and references therein). The full-width half-power beamwidths and main-beam efficiencies of the JCMT at 345 and 461 GHz are 14.3 ± 0.5 arcsec and 0.59 ± 0.03, and 10.9 ± 0.5 arcsec and 0.53 ± 0.05, respectively.

Table 3. CO data on IRC +10420.

line	Area	T_{peak}	σ	Velocity range		V_∞	V_{LSR}
				zero level	10% level		
	(K km s^{-1})	(K)	(K)	V_{LSR}	V_{LSR}	(km s^{-1})	(km s^{-1})
J1-0[1]	37 ± 0.5	0.62	0.024	30 - 120	37 - 117	40	77
J2-1	187 ± 1	3.17	0.036	29 - 121	36 - 116	40	76
J3-2	150 ± 1	2.70	0.09	30 - 120	39 - 116	38.5	77.5
J4-3	189 ± 6	3.81	0.25	30 - 117	40 - 114	37	77

[1]In agreement with Bachiller et al. (1988) where $\sigma = 0.14$ K.

The observations were made in the standard beam-switched mode, in which the secondary mirror was nutated so as to move the beam position on the sky ±60 arcsec in azimuth at 1 Hz. The telescope azimuth was modified every 60 s to place the source in alternate beam positions, thus effectively cancelling sky emission and baseline irregularities. The total integration times were short; 3 and 20 min at 345 and 461 GHz respectively. Half of this time was spent on the reference position. The data were processed after down conversion by an acousto-optical spectrometer with a channel spacing of 248 kHz. The data were subsequently smoothed over 21 channels, yielding effective spectral resolutions of 3.4 and 4.5 km s^{-1} at 345 and 461 GHz respectively. The calibration of the signals made use of hot and cold load and sky measurements to obtain the sky transmission and receiver noise temperatures. The final temperature scales should be accurate to within 25 per cent.

CO $J=1$–0 and 2–1 spectra at 115 and 230 GHz were taken simultaneously on 1994 December 28 with the 30-cm IRAM telescope at Pico Veleta, Spain. Two 1-MHz filterbanks were used to give channel spacings of 1.3 and 2.6 km s^{-1} at 230 and 115 GHz, respectively. The full-width half-power beam width and main-beam efficiencies at 115 and 230 GHz are 20.9 arcsec, 0.67 and 10.4 arcsec, 0.39, respectively. The integration times were 22 min for both frequencies, of which half was spent on the reference position. The spectra were initially calibrated by observing a hot and cold load. Final calibration was achieved by making comparisons with standard star observations. The temperatures (which are on a main-beam scale) are correct to within 10 per cent (1σ). These spectra and additional HCN(1–0) and SO(6_5–5_4) observations will be presented and discussed in more detail elsewhere (Blommaert, Groenewegen & Oudmaijer, in preparation).

3.1 Description of the spectra

The resulting spectra are plotted in Fig. 3. The line shapes are very different from the 'normal' flat-topped or parabolic profiles. The line profiles can be roughly characterized as flat-topped, with an excess emission on the blue side, or as parabolic, with a deficiency at the red side.

It seems that the asymmetry is less in the (1–0) line than in the (2–1) and (3–2) lines, suggestive of a stronger asymmetry of the envelope in the regions closer to the star. For reasons discussed below we prefer the interpretation of excess emission at blue-shifted velocities instead of red absorption. A lower signal-to-noise spectrum of SiO presented by Olofsson et al. (1982) shows the same shape, but these authors are rather careful, and describe the line profile as parabolic. The interpretation of the line profiles is difficult; it is noteworthy that many lines observed in IRC +10420 show a blue-to-red asymmetry.

The same asymmetry is observed for the OH maser, but an explanation for the extreme blue-to-red ratio is lacking (Giguere et al. 1976; Diamond, Norris & Booth 1983; Lewis, Terzian & Eder 1986; Nedoluha & Bowers 1992). Possible explanations are free–free absorption by ionized gas of the receding part of the OH maser, or an asymmetry in the coherent path lengths in the OH line-forming regions.

Parameters derived from the spectra are displayed in Table 3. The integrated area under the spectra, the peak temperature and the root mean square noise of the spectrum measured in the continuum (all on a main-beam scale) are presented. The velocity range of the spectrum is measured at the zero level and at the 10 per cent level of the spectrum, where the signal-to-noise ratio of the line is higher. Finally, in the last two columns, the outflow velocity and the central velocity, measured from the 10 per cent values, are listed.

The central velocity is in agreement with other determinations for the central velocity from other molecular species (Nercessian et al. 1989; Omont et al. 1993).

Note that the velocities measured from the zero level show a slight excess emission at larger blue-shifted velocities than at the redshifted velocities. This is apparent from the spectra as well; the decline to the zero level is shallower in the blue than in the red.

3.2 The gas mass-loss rates

The gas mass-loss rates can be calculated with equation (2) in Olofsson et al. (1993). Using $n_{He}/n_H = 0.1$ and a CO abundance relative to H_2 of 4×10^{-4}, we find mass-loss rates of 2.3×10^{-5} $(D/\mathrm{kpc})^2$ and 5.9×10^{-4} $(D/\mathrm{kpc})^2$ $M_\odot$ yr^{-1} for the (1–0) and (2–1) transitions, respectively. From equation (20) in Kastner (1992) we derive (using $f_{CO} = 4 \times 10^{-4}$ and $\alpha = 0.8$ for his scaling parameter) a mass-loss rate based on the (1–0) line of 2.0×10^{-5} $(D/\mathrm{kpc})^2$ $M_\odot$ yr^{-1}.

The results for the (1–0) line of Olofsson et al. and Kastner are similar, but there appears to be a difference of a factor 20 between the mass-loss rates obtained from the

(1–0) and the (2–1) lines. Kastner (1992) warns that for mass-loss rates much in excess of 10^{-5} $M_\odot$ yr^{-1} no simple formula can be used. Detailed modelling of such data is required to obtain more reliable gas mass-loss rates from the CO emission.

3.3 The outflow velocity

The large observed outflow velocity of 40 km s^{-1} is much larger than the observed mean outflow velocity for AGB stars, which is 15 km s^{-1} (Olofsson 1993). In fact, this offers an indirect argument against the post-AGB hypothesis for IRC +10420.

The velocity at infinity of an expanding dust shell can be estimated by assuming that the outflow is a wind radiatively driven by photon pressure on dust grains. Habing, Tignon & Tielens (1994) studied radiatively driven winds for mass-losing objects. As an approximation for the outflow velocity they find $v_{esc} \propto L^{0.3} \times \Psi^{0.5}$. In their fig. 8, we find that for mass-loss rates of 10^{-4} $M_\odot$ yr^{-1}, $L = 10^4$ $L_\odot$ and $\Psi = 0.008$, the expansion velocity is 16 km s^{-1}. When taking the same dust-to-gas ratio but the maximum possible AGB luminosity, one obtains an expansion velocity of only 26 km s^{-1}, which is indeed close to the maximum observed outflow velocities in AGB stars. Very high dust-to-gas ratios are needed to account for the observed expansion velocity of IRC +10420; if one increases Ψ to 0.02 the luminosity should be of order 46 000 $L_\odot$. Instead, an outflow velocity of 40 km s^{-1} is obtained for $L = 212\,000$ $L_\odot$ and $\Psi = 0.008$, or $L = 464\,000$ $L_\odot$ and $\Psi = 0.005$. These luminosities are typical for massive supergiants.

If IRC +10420 is a post-AGB object, the observed expansion velocity can thus only be explained if IRC +10420 was a very luminous AGB star with an extremely high dust-to-gas ratio. For normal values of the dust-to-gas ratio, the luminosities are as expected for massive stars.

4 FITTING THE SPECTRAL ENERGY DISTRIBUTION

In this section we model the resulting spectral energy distribution (SED) of IRC +10420 with the dust radiative transfer model of Groenewegen (1993). In this model the radiative transfer equation and the equation of thermal equilibrium are solved simultaneously for the dust in spherical geometry.

The input for the fit is the 1992 SED that is constructed in Section 2: other relevant parameters for the fitting are the outflow velocity of the envelope, taken to be 40 km s^{-1}, from the CO spectra. The extinction towards IRC +10420 is the sum of the interstellar and the circumstellar extinctions. The models have been corrected for an interstellar extinction of $A_V \approx 5$, as determined by Oudmaijer (1995) from the strength of the 'Diffuse Interstellar Bands', and in agreement with the value determined by J93 for the interstellar extinction from polarization measurements. A 7000-K blackbody is used to represent the stellar continuum. We chose a blackbody instead of a model atmosphere because it is shown in the above sections that the temperature of IRC +10420 is not well determined. A blackbody of 7000 K appears to be a good compromise, considering the uncertainties in the temperature of IRC +10420 and the associated extinction as discussed earlier.

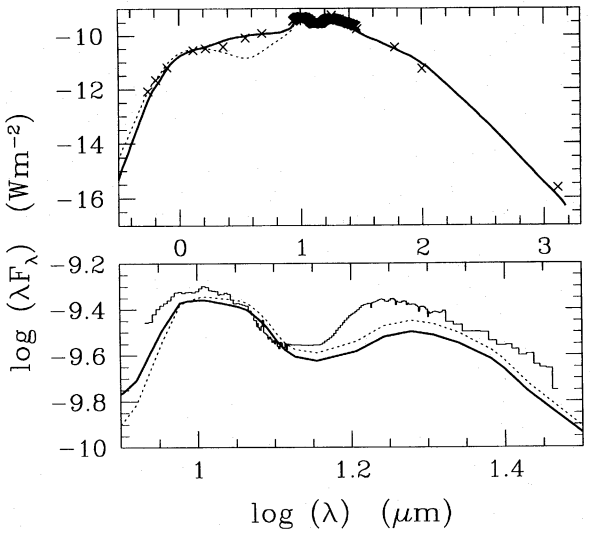

Figure 4. Model fits through the energy distribution of IRC +10420. The crosses represent the '1992' set of data discussed in the text. The dashed line is the model fit using a single-shell model, while the solid line represents the model fit, where an additional hot circumstellar component is introduced. The lower panel shows the LRS spectral range in more detail. The histogram represents the combined LRS spectrum and KAO photometry.

The shape of the SED is fully determined by the effective temperature of the central star, the dust temperature at the inner radius, the dust optical depth at a reference wavelength and the relative variation with wavelength of the extinction coefficient, Q_λ. For a particular choice of $T_{\rm eff}$ and Q_λ, the dust optical depth and $T_{\rm inner}$ are derived. These parameters are independent of the assumed distance. Furthermore, L/D^2 is independent of distance.

The relation between the dust optical depth and physical quantities is $\tau_\lambda \sim (\dot{M}\Psi\kappa_\lambda)/(R_* r_{\rm inner} v)$, where $\dot{M}$ is the total mass-loss rate, Ψ is the dust-to-gas ratio, κ_λ is the dust opacity [$\kappa_\lambda = 3Q_\lambda/(4a\rho_{\rm d})$, with Q_λ being the absorption efficiency, a the dust grain size and $\rho_{\rm d} = 2$ g cm^{-3}, the adopted specific density of the dust grains], R_* is the stellar radius in solar radii, $r_{\rm inner}$ is the inner dust radius in stellar radii and v is the expansion velocity, assumed to be constant, of the envelope.

The calculations are performed in the small particle limit so that Q_λ/a is independent of a, and scattering can be neglected. The radiative silicate dust opacity was taken from Volk & Kwok (1988), scaled to an absolute value of the opacity of $\kappa_{60\mu m} = 150$ cm^2 g^{-1}. We assume a dust-to-gas ratio of 0.005. The explicit distance dependence is introduced through the stellar radius ($R_* \sim \sqrt{L} \sim D$). Hence, both the mass-loss rate and the flow time-scales in the envelope scale linearly with distance.

4.1 A single shell

At first we attempted to fit the SED of IRC +10420 with a single dust shell. It turns out, however, that this does not provide a good fit to the data. The best fit that we obtained

fits the cool part of the envelope (i.e. $\lambda > 10$ μm), but at the shorter wavelengths the SED could not be fitted; at wavelengths shorter than 4 μm the model fit lies significantly above the photometry, while the model fit lies below the observations in the range 4–16 μm.

The detailed fits to the LRS and KAO spectra are important constraints to use to arrive at the fit parameters; the underlying dust continuum peaks at $\lambda \approx 3000/T_{\rm inner}$ μm, which for the values of interest is located in the LRS wavelength region, and the excitation of the 9.8- and 18-μm silicate features. For $T_{\rm inner} \lesssim 290$ K the peak of the SED is shifted so far to the red that the 18-μm feature is much stronger than the 9.8-μm feature. For $T_{\rm inner} \gtrsim 600$ K the reverse is true. The combination of fitting the broad-band SED, the LRS and the KAO spectra leads to a best-fitting value of $T_{\rm inner} = 400$ K.

This best fit, with parameters $T_{\rm inner} = 400$ K (with the inner radius at 486 stellar radii), $\dot{M} = 1.8 \times 10^{-4}$ (D/kpc) $M_\odot$ yr^{-1} and $L = 21\,700$ (D/kpc)^2 $L_\odot$ is shown in Fig. 4 as a dashed line. The flow time-scale, that is, the kinematic age from the stellar surface to the inner radius, is 27 (D/kpc) yr.

For distances in the range 3.5–5 kpc, the mass-loss rate derived from the CO (1–0) line and the model fitting agree to better than a factor of 2 and range from about 5×10^{-4} $M_\odot$ yr^{-1} at 3.5 kpc to about 10^{-3} $M_\odot$ yr^{-1} at 5 kpc.

We assume an r^{-2} density distribution and an outer radius that is determined by the radial distance where the dust temperature has dropped to 20 K. For the calculated models the outer radius is located at about 4.1×10^5 stellar radii, or at a time-scale of 2.4×10^4 (D/kpc) yr. Thus, the shell would contain about 40 solar masses if the stellar is located at a distance of 3.5 kpc. Kastner & Weintraub (1995) performed near-infrared coronographic imaging of IRC +10420, and found that the scattering dust extends out to at least 9 arcsec. This corresponds to about 1000 (D/kpc) yr with an expansion velocity of 40 km s^{-1}. If the outer radius of the dust shell is indeed smaller than the value used in the calculations, the period of high mass loss has lasted only a limited amount of time.

As far as we know there has been only one other attempt to fit the SED of IRC +10420. Hrivnak, Kwok & Volk (1989) fit a single shell, and noticeable in their fig. 7 is that the near-infrared part is not fitted. In that wavelength region the model is almost photospheric, and lies significantly below the observed SED. Their result hints already at the fact that the SED cannot be fitted with one shell, but that an additional hotter component must be included, although this is not obvious since the SED does not have a 'triple-peaked' behaviour.

The hot dust is responsible for the energy emitted in the near-infrared part of the SED, while cool dust emits in the far-infrared part of the SED. A two-component fit is not unusual; Trams (1991) finds that significant amounts of dust in the envelopes of post-AGB stars are located in a hot shell or disc, with colour temperatures of the order of 1000 K.

4.2 Two-shell model

Considering the above, we next tried to fit the SED with a two-component model; for reasons of simplicity we take the inner radius of the best-fitted cool shell in the above section to be equal to the outer radius of the inner shell. The dust temperature at the inner radius of the inner shell is taken to be the typical condensation temperature of silicate dust, i.e. 1000 K.

By keeping the inner and outer radii fixed, we performed interations until the best fit was obtained. The inclusion of an extra shell considerably improves the fits; the best fit is shown in Fig. 4 as a solid line. The inner radius lies at 86 stellar radii, $\dot{M}$ (cool) $= 2.0 \times 10^{-4}$ (D/kpc) $M_\odot$ yr^{-1}, and $\dot{M}$ (hot) $= 1.4 \times 10^{-5}$ (D/kpc) $M_\odot$ yr^{-1}, $L = 23\,400$ (D/kpc) $L_\odot$. Note that the best fit has slightly different values for the luminosity and the mass-loss rate of the cool component compared with the single shell model. The A_V of the cool envelope as we calculate is ~ 2, independent of the assumed distance to the object, which together with the interstellar $A_V = 5$ yields 7-mag extinction, as observed. The hot envelope, if spherical, introduces an extra A_V of 0.9.

5 DISCUSSION

5.1 The cool shell

The kinematic age of the cool shell is 27 (D/kpc) yr. 20 years ago, the shape and magnitude of the infrared excess emission owing to dust was comparable to the present day energy distribution. If IRC +10420 is a post-AGB star this would imply that it would be at a distance of < 1.6 kpc, since the maximum luminosity of any AGB progenitor is $\sim 55\,000$ $L_\odot$, corresponding to the maximum possible mass of a white dwarf, 1.44 $M_\odot$ (Iben & Renzini 1983). A cool shell dynamical age of < 45 yr implies that the SED of 1974 would be very different from how it is now, most notably the V band would suffer a much larger extinction than observed now since the dust would be closer to the star. This problem is less severe if IRC +10420 was a massive object located at several kpc, since the age of the shell increases with distance.

The work of Gottlieb & Liller (1978) allows us to compare the photometry with observations from the beginning of this century. These authors measured the photographic magnitude of IRC +10420, converted to the Johnson B band, from a collection of Harvard photographic plates, and present the photometric evolution of IRC +10420 from 1900 to 1978. In the period 1900–1920, where the observational errors are largest, they find that the magnitude of IRC +10420 was scattered between $B = 14$ and 15, but, that since 1920, B decreased from ~ 15.2 to 13.8 in 1978.

The brightening in B can be caused by either an increase in temperature with a constant extinction or by the decrease in circumstellar extinction, or a combination of both. It will be useful to calculate a grid of models with the fit parameters derived in this paper in order to investigate the evolution of the spectral energy distribution as a function of time, distance and temperature. We suffice here, however, with a simple consideration.

As no U- or B-band photometry has been obtained since 1978, we restrict the following discussion to the difference in B between 1920 and 1978, which is 1.4 mag. Assuming that the increase in flux at the B band is entirely owing to the dilution of the circumstellar shell, this translates into a change in circumstellar B extinction of $\Delta A_B = 1.4$. Assuming a wavelength-dependent extinction following a Savage & Mathis (1979) curve, $\Delta A_V = 1.4$ corresponds to $\Delta A_V = 1.1$,

hence $\Delta\tau_V \sim 1$.

The optical depth at V from the model fit for the cool shell is ~ 2. The change in A_V between 1978 and 1992 is hard to estimate, but is not likely to be large (cf. Section 2). Let us assume that $\tau_V = 2$ in 1978. The optical depth at the V band should then be 3 in 1920. Because $\tau_V \propto 1/r_{\rm inner} = 1/v(t-t_0)$, one has $3/2 = (1978-t_0)/(1920-t_0)$, from which it follows that t_0 corresponds to the year 1804. The kinematic age of the dust shell, $t-t_0$, would therefore be 184 yr in 1978 corresponding to ~ 200 yr now. This simple calculation does not take any temperature changes into account: had temperature of IRC +10420 increased in the same period, the decrease in circumstellar extinction would be smaller, and the kinematic age of the inner radius larger. The value of 200 yr is in reasonable agreement with the value inferred from the model fits. For a distance to IRC +10420 of 3.5–5 kpc the kinematic ages of the present-day shell are 95 and 135 yr, respectively. In any case, the possibility of IRC +10420 being a post-AGB star located closer than 1.6 kpc from Earth is effectively ruled out when applying this argument.

One could, however, argue that the cool dust is located in a *disc*, oriented pole-on with respect to the observer. In that case the relatively small change in extinction is naturally explained by the fact that most material is not located in the line of sight. In Section 3, an indication of deviations from spherical symmetry in the envelope of IRC +10420 was already presented, there are, however, problems with a strong asymmetry of the cool shell.

The shape of the envelope, as traced by the dust, CO rotational–vibrational lines, and the OH maser, is roughly an oblate ellipsoid, as Nedoluha & Bowers (1992) find from high-resolution maps in OH. The presence of P Cygni profiles in the high-resolution spectra in the CO 4.6-μm rotational–vibrational lines, which trace cool gas (Fix & Cobb 1987), suggests that deviations from spherical symmetry are probably not large. In addition, if the cool dust, where the CO (sub)mm emission is likely to originate, is strongly asymmetric and oriented pole-on, high outflow velocities would not be expected.

5.2 The hot dust component

The model fitting required the presence of a hot dust component, responsible for emission at the near-infrared wavelength bands. The kinematic age of the inner radius of this shell is only 5 yr kpc^{-1}.

This could imply that a recent outflow is responsible for the excess emission. 20 years ago, the near-infrared excess was already present when Humphreys et al. (1973) observed IRC +10420 spectroscopically, but they did not find spectroscopic evidence for an outflow.

Perhaps it is more likely that the hot component reflects the presence of a circumstellar disc around IRC +10420, as already invoked by J93 on the basis of extinction and polarization arguments. A Keplerian rotating disc surrounding IRC +10420 is a likely assumption to account for the observed near-infrared excess.

Hot discs around evolved stars have been found before: Trams 1991, Waters et al. 1993a, van Winckel, Waelkens & Waters 1995 discuss several examples of evolved (post-AGB candidate) stars with the same near-infrared properties. These authors find an almost one-to-one correlation between the presence of hot dust (i.e. circumsystem disc) and binarity of the star (Waters et al. 1993a, and more recently for HD 101584, Bakker 1995; van Winckel et al. 1995). In all cases, the secondary object is not observed, and may be a low-mass main-sequence object, or an initially more massive object, which is now a white dwarf.

IRC +10420 may be the member of a binary system: if this is the case, then radial velocity variations should be observed. It is, however, hard to actually disentangle the contribution of the velocity shift owing to binary motion from the contribution of the spectral variability that may be caused by stellar pulsations (see Oudmaijer et al. 1995). The possibility that IRC +10420 is a member of a binary system cannot be excluded with the present data.

6 CONCLUDING REMARKS

In this paper we have presented a study of the spectral energy distribution and mass-loss history of the peculiar hypergiant IRC +10420. The results can be summarized as follows.

(i) The spectral energy distribution of IRC +10420 has changed significantly over the last 20 years. While the V magnitude remained constant during this period, the (photospheric) J and K bands increased by 0.75 mag. We argue that the temperature of IRC +10420 has increased by about 1000 K.

(ii) Observations of the CO rotational transitions reveal complicated line profiles, where there is an excess emission at the blueshifted side of the emission lines. The red-to-blue asymmetry is found in many lines tracing different line-forming regions (Hα, SiO, OH), and suggests that the circumstellar envelope is slighty asymmetric over a large range of distances to the star.

(iii) The spectral energy distribution of IRC +10420 cannot be fitted with one component. An additional hot dust component responsible for the observed excess emission at the near-infrared wavelengths was added to the model fit, giving satisfactory fits. The hot dust component is identified with a disc.

(iv) The mass-loss rate of IRC +10420, as determined from the CO (1–0) lines and the model to the entire spectral energy distribution, is found to be of the order of 5×10^{-4} $M_\odot$ yr^{-1} for a distance of 3.5 kpc.

(v) We have presented evidence that IRC +10420 is *not* a post-AGB star. This is based on two arguments. First, the observed high outflow velocities in CO can only be reached for the brightest possible post-AGB objects with extremely high dust-to-gas ratios. Secondly, the kinematic age of the inner radius of the cool shell is too low to explain the fact that the V magnitude of IRC +10420 has remained essentially constant over the last 20 years and the fact that the B magnitude brightened only by 1.4 mag in the period between 1920 and 1978.

ACKNOWLEDGMENTS

Rens Waters is thanked for fruitful discussions. RSO received financial support under grant no. 782-372-031 from the Netherlands Foundation for Research in Astronomy

(ASTRON), which receives its funds from the Netherlands Organisation for Scientific Research (NWO). The James Clerk Maxwell Telescope is operated by The Observatories on behalf of the Particle Physics and Astronomy Research Council (PPARC) of the United Kingdom, the Netherlands Organization for Scientific Research and the National Research Council of Canada. The Observatorio del Teide on the island of La Palma is operated by the Instituto de Astrofísica de Canarias, Tenerife. This research has made use of the SIMBAD data base operated at CDS, Strasbourg, France.

REFERENCES

Alonso A., Arribas S., Martinez-Roger C., 1994, A&AS, 107, 365
Assendorp R., Bontekoe Tj. R., de Jonge A. R. W., Kester D. J. M., Roelfsema P. R., Wesselius P. R., 1995, A&AS, 110, 395
Bachiller R., Gómea-González J., Bujarrabal V., Martin-Pintado J., 1988, A&A, 196, L5
Bakker E. J., 1995, PhD thesis, University of Utrecht
Craine E. R., Schuster W. J., Tapia S., Vrba F. J., 1976, ApJ, 205, 802
Diamond P. J., Norris R. P., Booth R. S., 1983, A&A, 124, L4
Fix J. D., Cobb M. L., 1987, ApJ, 312, 290
Giguere P. T., Woolf N. J., Webber J. C., 1976, ApJ, 207, L195
Gottlieb E. W., Liller W., 1978, ApJ, 225, 488
Groenewegen M. A. T., 1993, PhD thesis, University of Amsterdam, Chapter 5
Habing H. J., Tignon J., Tielens A. G. G. M., 1994, A&A, 286, 523
Hrivnak B. J., Kwok S., Volk K. M., 1989, ApJ, 346, 265
Humphreys R. M., 1991, in van der Hucht K. A., Hidayat K., eds, Wolf-Rayet stars and interrelations with other massive stars in galaxies. Kluwer, Dordrecht, p. 485
Humphreys R. M., Strecker D. W., Murdock T. L., Low F. J., 1973, ApJ, 179, L53
Iben I., Renzini A., 1983, ARA&A, 21, 271
Johnson H., Mitchell R., 1975, Rev. Mex. Astron. Astrofis., 1, 299
Jones T. J. et al., 1993, ApJ, 411, 323 (J93)
Kastner J. H., 1992, ApJ, 401, 337
Kastner J. H., Weintraub D. A., 1995, ApJ, 452, 833
Koornneef J., 1993, A&A, 128, 84
Kurucz R. L., 1979, ApJS, 40, 1
Kwok S., 1993, ARA&A, 31, 63
Lewis B. J., Terzian Y., Eder J., 1986, ApJ, 302, L23
Matthews H. E., 1995, Guide for the Prospective User of the James Clerk Maxwell Telescope
Nedoluha G. E., Bowers P. F., 1992, ApJ, 392, 249
Nercessian E., Guilloteau S., Omont A., Benayoun J. J., 1989, A&A, 210, 225
Ney E. P., Strecker D. W., Gehrz R. D., 1973, ApJ, 180, 809
Olofsson H., 1993, in Schwarz H. E., ed., ESO Conference and Workshop Proceedings No. 46, Second ESO/CTIO workshop Mass loss on the AGB and beyond. ESO, Garching, p. 330
Olofsson H., Johansson L. E. B., Hjalmarson A., Rieu N. Q., 1982, A&A, 107, 128
Olofsson H., Eriksson K., Gustafsson B., Carlström U., 1993, ApJS, 87, 267
Omont A., Lucas R., Morris M., Guilloteau S., 1993, A&A, 267, 490
Oudmaijer R. D., 1995, in Watt G. D., Williams P. M., eds, Conf. Circumstellar Matter 1994. Kluwer, Dordrecht, p. 325
Oudmaijer R. D., Geballe T. R., Waters L. B. F. M., Sahu K. C., 1994, A&A, 281, L33
Oudmaijer R. D., Waters L. B. F. M., Geballe T. R., 1995, in Oudmaijer R. D., PhD thesis, University of Groningen, Chapter 10
Savage B. D., Mathis J. S., 1979, ARA&A, 17, 73
Schaller G., Schaerer D., Meynet G., Maeder A., 1992, A&AS, 96, 269
te Lintel-Hekkert P. T. L., Chapman J. M., Zijlstra A. A., 1992, ApJ, 390, L23
Trams N. R., 1991, PhD thesis, University of Utrecht
van der Hulst J. M., Terlouw J. P., Begeman K. G., Zwitser W., Roelfsema P. R., 1992, in Worall D. M., Biemesderfer C., Barnes J., eds, ASP Conf. series no. 25, Astronomical Data Analysis Software and Systems I, p. 131
van Winckel H., Waelkens C., Waters L. B. F. M., 1995, A&A, 293, L25
Volk K. M., Kwok S., 1988, ApJ, 331, 435
Walmsley C. M., Chini R., Kreysa E., Steppe H., Forveille T., Omont A., 1991, A&A, 248, 555
Waters L. B. F. M., Waelkens C., Trams N. R., 1993a, in Schwarz H. E., ed., ESO Conference and Workshop Proceedings No. 46, Second ESO/CTIO workshop on Mass Loss on the AGB and Beyond. ESO, Garching, p. 298
Waters L. B. F. M., Waelkens C., Mayor M., Trams N. R., 1993b, A&A, 269, 242
Wesselius P. R., de Jonge A. R. W., Kester D. J. M., Roelfsema P. R., 1992, in Encrenaz T., Kessler M. F., eds., Infrared Astronomy with ISO. Nova Science Publishers Inc. NY, p. 509